Research Square

Preprints are preliminary reports that have not undergone peer review.
They should not be considered conclusive, used to inform clinical practice,
or referenced by the media as validated information.

Quantitative Image-Based Characterisation of Moisture-Induced Asphalt Stripping: Method Validation and Material Effects

Yalcin Karakaya

yalcin.karakaya@cbu.edu.tr

Manisa Celal Bayar University

Ayhan Yucel

Adnan Menderes University

Dilay Uncu

Manisa Celal Bayar University

Article

Keywords: Asphalt stripping, Moisture susceptibility, Digital image analysis, Aggregate morphology, Image segmentation, SBS-modified binder

Posted Date: October 8th, 2026

DOI: https://doi.org/10.21203/rs.3.rs-11292273/v1

License: This work is licensed under a Creative Commons Attribution 4.0 International License.
Read Full License

Additional Declarations: No competing interests reported.

Quantitative Image-Based Characterisation of Moisture-Induced Asphalt Stripping: Method Validation and Material Effects

Yalcin Karakaya[1*], Ayhan Oner Yucel[2], Dilay Yildirim Uncu[1]

[1]Department of Civil Engineering, Manisa Celal Bayar University, Manisa 45140, Türkiye

[2]Department of Civil Engineering, Aydin Adnan Menderes University, Aydin 09010, Türkiye

***Corresponding author:**

Yalcin Karakaya

Department of Civil Engineering

Manisa Celal Bayar University

Manisa 45140, Türkiye

E-mail: yalcin.karakaya@cbu.edu.tr

ORCID ID: 0000-0003-1036-7941

Author ORCIDs:

Yalcin Karakaya: [0000-0003-1036-7941]

Ayhan Oner Yucel: [0000-0001-5888-2809]

Dilay Yildirim Uncu: [0000-0001-8660-2114]

Abstract

Conventional visual assessment of asphalt stripping is inherently subjective. This study developed and evaluated a digital image analysis framework for loose asphalt-coated aggregates subjected to modified static immersion and boiling water conditioning. Each procedure comprised 96 factorial treatment combinations, evaluated repeatedly at three conditioning stages, incorporating binder system and short-term ageing, aggregate source, particle size and morphology, and exposure to sodium chloride. Standardised image acquisition was combined with CIELAB colour space segmentation, using fixed, source-specific classification criteria derived from separate calibration images. Validation against manually delineated reference masks yielded a mean absolute error of 4.68 percentage points and a concordance correlation coefficient of 0.946. Stripping increased with conditioning duration and was greater in a 4% sodium chloride solution. Among the investigated material contrasts, binder system showed the largest adjusted difference in both procedures; greater coating loss was also associated with ageing, the investigated basalt aggregate, smaller particles, and cubical-rounded particles relative to cubical-angular particles. The

two conditioning procedures produced consistent relative differentiation among material combinations but were not quantitatively interchangeable. The proposed framework provides a validated quantitative method for measuring visible asphalt coating loss and characterising material and conditioning effects under standardised imaging conditions.

Keywords: Asphalt stripping; Moisture susceptibility; Digital image analysis; Aggregate morphology; Image segmentation; SBS-modified binder

1. Introduction

Moisture-induced damage remains one of the most persistent durability concerns in asphalt pavements, as water progressively weakens the bond between the asphalt binder and mineral aggregate, leading to stripping, loss of mixture integrity, and accelerated pavement deterioration. At the material scale, moisture damage may involve adhesive failure at the asphalt–aggregate interface and cohesive failure within the binder or mastic; these mechanisms are influenced by material properties and moisture exposure conditions [1,2]. When water reaches the asphalt–aggregate interface, it can weaken the adhesive bond and promote debonding of the asphalt binder from the aggregate surface [3]. The resulting deterioration reduces mixture strength and stiffness, adversely affecting pavement service life [4]. Consequently, understanding the material factors that govern asphalt–aggregate adhesion is essential for improving the moisture resistance and long-term durability of asphalt pavements.

Aggregate mineralogical composition and surface physicochemical properties can influence asphalt–aggregate adhesion and its resistance to moisture-induced debonding [5–7]. Different aggregate sources can exhibit different adhesion behaviour in the presence of moisture; limestone has shown better asphalt–aggregate adhesion and moisture resistance than basalt in specific material systems [8,9]. While surface texture has been linked to aggregate surface free energy [10], aggregate angularity has been associated with asphalt–aggregate interphase characteristics and mixture water stability [11]. Particle size can also influence moisture susceptibility; it has been reported that decreasing aggregate size increases the potential for stripping [12]. In addition, higher proportions of flat and elongated particles have been associated with greater void content and reduced moisture resistance [13].

Polymer modification, particularly with SBS, alters binder rheology and elasticity, and can also affect binder cohesion, asphalt–aggregate adhesion, and resistance to moisture damage [14–16]. Ageing further complicates this response, as it changes binder stiffness, surface free energy, wettability, and asphalt–aggregate bond characteristics. Previous investigations have shown that ageing can modify cohesive and adhesive behaviour and alter moisture resistance [17–19]. Its influence may depend on the binder–aggregate combination and on whether ageing occurs before or after the binder coats the aggregate surface [17].

Conventional loose mixture procedures, including static immersion and boiling water tests, are widely used because they are relatively simple, rapid, inexpensive, and allow direct observation of

asphalt film loss from aggregate surfaces. However, retained asphalt coating is traditionally estimated visually, making the assessment susceptible to operator judgement, lighting conditions, aggregate colour, and other observational factors [20,21]. Digital image processing techniques have therefore been introduced to quantify exposed aggregate and retained asphalt coating and to reduce the subjectivity associated with visual assessment [20–23]. From a measurement perspective, the challenge is not only to automate visual classification, but also to consistently convert variations in aggregate surface appearance into a quantitative stripped area measurement and to characterise its agreement with an independent reference. Reliable quantitative image analysis requires clearly defined image-processing procedures and appropriate evaluation of measurement performance by comparison with independent or established reference measurements, including assessment of accuracy and repeatability [24,25].

The methodological challenge extends beyond simply replacing subjective visual assessment with automated pixel classification. For image-derived stripped areas to be used for quantitative comparison of material systems, the measurement procedure should be established independently of the data used to evaluate its performance. Previous image-based stripping studies have largely focused on automating visual assessment or evaluating selected material and conditioning variables [20–22,26,27], whereas calibration, independent measurement validation, and subsequent analysis of material effects have received less attention within a common experimental framework.

The present study addresses this issue through a two-stage framework for measurement and application. First, a standardised image acquisition and CIELAB segmentation procedure was established using dedicated calibration images and independently evaluated against manually delineated reference masks using measurement error, concordance, and spatial overlap metrics. Second, after fixing the aggregate source-specific classification criteria, the procedure was applied, without image-specific adjustment, to a structured factorial experiment with 96 treatment combinations for each of the two moisture-conditioning procedures. This separation between method calibration, independent validation, and experimental application allowed the performance of the image-based measurement procedure to be evaluated before the resulting measurements were used to characterise material and conditioning effects.

The objectives of the study are to (i) establish and independently validate an image-based procedure for quantitatively measuring visible asphalt coating loss; (ii) apply this procedure to quantify the effects of binder system and ageing, aggregate type, particle size and morphology, sodium chloride exposure and conditioning duration; and (iii) determine whether static immersion and boiling water conditioning provide consistent relative differentiation among the investigated material combinations.

2. Materials and Methods

2.1.Materials

Two asphalt binder systems were used in the experimental programme: a neat 50/70 penetration-grade bitumen and a plant-produced polymer-modified binder (PMB) classified as PG 76-16.

According to the supplier, the PMB contained 4% styrene–butadiene–styrene (SBS) polymer by binder mass. The SBS-modified binder was not produced by modifying the neat 50/70 binder used in this study; therefore, the comparison between the two materials reflects a contrast between binder systems rather than the isolated effect of SBS modification. Both binders were evaluated in unaged and short-term aged conditions. Short-term ageing was carried out using the Rolling Thin Film Oven (RTFO) procedure in accordance with ASTM D2872 at 163 °C for 85 min. The physical properties of the binders before and after RTFO ageing are summarised in Table 1.

Table 1. Physical properties of the two investigated binder systems before and after RTFO ageing.

Property	Test method	Neat binder		SBS-modified binder	
		Unaged	RTFO-aged	Unaged	RTFO-aged
Penetration (0.1 mm)	ASTM D5/D5M	58	40	39	31
Specific gravity	ASTM D70/D70M	1.036	1.045	1.028	1.034
Softening point (°C)	ASTM D36/D36M	52	58	76	82
Flash point (°C)	ASTM D92	>300	>300	>300	>300
Ductility at 25 °C, 5 cm/min (cm)	ASTM D113	>100	70	>100	92
Rotational viscosity at 135 °C (mPa·s)	ASTM D4402/D4402M	550	995	2438	3025

Note: RTFO = Rolling Thin Film Oven; SBS = styrene–butadiene–styrene.

Two aggregate types, limestone and basalt, were obtained from commercial quarries in Manisa and Izmir, respectively. Table 2 presents the properties of the coarse and fine fractions. Basalt exhibited higher water absorption than limestone in both size fractions, whereas the lower Los Angeles abrasion value measured for the coarse basalt aggregate indicated greater resistance to mechanical wear.

Table 2. Physical properties of the limestone and basalt aggregates.

Property	Test method	Limestone		Basalt	
		Coarse	Fine	Coarse	Fine
Bulk specific gravity (oven-dry)	ASTM C127 / ASTM C128	2.706	2.684	2.721	2.696
Apparent specific gravity	ASTM C127 / ASTM C128	2.733	2.704	2.803	2.774
Water absorption (%)	ASTM C127 / ASTM C128	0.365	0.276	1.075	1.043
Los Angeles abrasion (%)	ASTM C131/C131M	27	–	16	–

Note: 'Coarse' and 'fine' refer to the conventional aggregate fractions used for material characterisation and should not be confused with the 'large' and 'small' particle size groups used in the stripping experiments. Los Angeles abrasion was determined only for the coarse aggregate fraction.

2.2.Experimental Design

The experimental programme was designed to evaluate the effects of the binder system, binder ageing, aggregate type, particle size, aggregate morphology, and conditioning medium on moisture-induced stripping. The corresponding factor levels are summarised in Table 3. The full

factorial combination of these six factors produced 96 treatment combinations for each moisture-conditioning procedure. One experimental unit was prepared for each treatment combination in each procedure, yielding 96 independent experimental units for static immersion and 96 for boiling-water conditioning. Each experimental unit was evaluated repeatedly at three successive conditioning stages.

Table 3. Experimental factors and levels considered in the study.

Factor	Levels
Binder system	Neat 50/70; commercial SBS-modified PG 76-16
Binder ageing condition	Unaged, RTFO-aged
Aggregate type	Limestone, basalt
Particle size	Small (6.3–9.5 mm), large (9.5–12.5 mm)
Aggregate morphology	Cubical-angular (CA), cubical-rounded (CR), flaky-angular (FA)
Conditioning medium	NaCl-free water, 4% NaCl solution

Note: RTFO = Rolling Thin Film Oven; SBS = styrene–butadiene–styrene.

Aggregate morphology was represented by three experimentally defined conditions: cubical-angular (CA), cubical-rounded (CR) and flaky-angular (FA). A flaky-rounded condition was not included because the rounding procedure could not be applied to flaky particles without substantially altering their characteristic geometry. Consequently, shape and angularity were not treated as fully crossed, independent variables. Instead, two prespecified morphological contrasts were used: CR versus CA to evaluate a morphological contrast related to angularity, and FA versus CA to evaluate a morphological contrast related to shape.

The stripped area was repeatedly measured on the same experimental unit after successive conditioning periods of 1, 3, and 7 days of static immersion, and 10, 30, and 60 minutes of boiling water conditioning. Conditioning duration was therefore treated as a repeated within-specimen measure rather than as an additional independent treatment factor.

2.3.Aggregate Morphology Preparation, Classification and Characterisation

Two particle size fractions were considered: small particles passing the 9.5 mm sieve and retained on the 6.3 mm sieve, and large particles passing the 12.5 mm sieve and retained on the 9.5 mm sieve. Particle shape was assessed in accordance with ASTM D4791, using a dimensional ratio of 5:1. Particles exceeding this criterion were designated as flaky (flat and/or elongated), whereas the remaining particles were designated as cubical. Rounded particles were produced from the original limestone and basalt aggregates using a modified Los Angeles drum polishing procedure. For each treatment, 2.5 kg of aggregate was placed in the drum with 3 kg of clean silica sand. No steel ball charge was used, and the drum was operated at approximately 30 rpm for 2,000 revolutions. After treatment, the abrasive medium and generated fines were removed by sieving, and particles remaining within the specified size fraction were retained. Controlled abrasion in a Los Angeles abrasion apparatus has similarly been used to induce morphological changes in aggregate particles for subsequent image-based characterisation [28].

Morphological changes produced by the polishing procedure were quantified using two-dimensional image analysis. Angular and rounded particles from both aggregate sources and both particle size fractions were photographed from a fixed distance under controlled lighting against a white background. Between approximately 30 and 110 particles were analysed for each combination of aggregate type, particle size and morphology. The images were cropped while preserving complete particle boundaries, converted to greyscale, and processed to enhance the contrast between the particles and the background. Adaptive thresholding was then applied to obtain binary masks of the particles (see Figure 1). Image-based analysis has been widely used for quantitative characterisation of aggregate morphology, including particle shape and angularity [28,29].

For each binary particle mask, particle area (A), perimeter (P), convex hull area (A_c), convex hull perimeter (P_c), and major and minor axis lengths (L_{maj} and L_{min}) were obtained in MATLAB. Five complementary two-dimensional morphological descriptors were subsequently calculated: circularity ($4\pi A/P^2$), solidity (A/A_c), convexity (P_c/P), aspect ratio (L_{maj}/L_{min}), and roundness $\left[4A/(\pi L_{maj}^2)\right]$. Circularity, solidity, convexity and aspect ratio have previously been used to quantitatively characterise particle morphology in binary images [30,31].

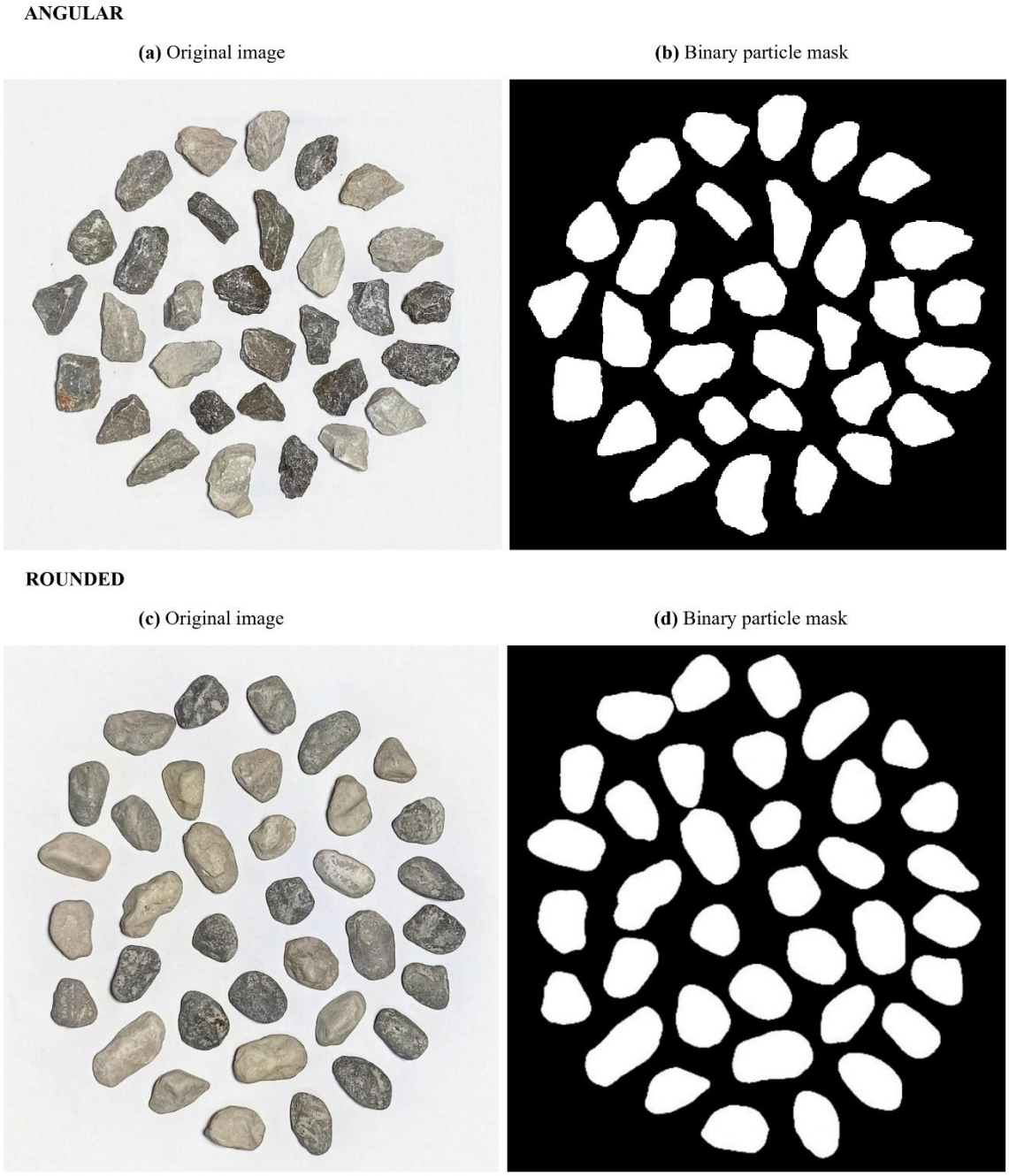


Fig. 1 Representative aggregate images and corresponding binary masks used for two-dimensional morphological characterisation: (a) original image of angular particles; (b) corresponding binary particle mask; (c) original image of rounded particles after the modified drum polishing treatment; and (d) corresponding binary particle mask

Circularity is influenced by both boundary irregularity and overall particle shape and therefore does not, by itself, represent angularity. Similarly, solidity and convexity provide related but complementary information: solidity reflects the difference in area between the particle and its convex hull, whereas convexity reflects irregularities along the particle boundary. Aspect ratio

primarily characterises elongation rather than corner angularity, while roundness provides an additional measure of particle compactness in projection. Previous morphometric analyses have likewise shown that circularity, convexity, and solidity respond to changes in grain roundness, whereas aspect ratio provides complementary information on overall particle shape [30]. Accordingly, the selected descriptors were used collectively to characterise the overall morphological changes produced by polishing rather than to represent angularity with a single index. The calculated morphological descriptors for angular and rounded limestone and basalt particles are summarised in Table 4.

Table 4. Two-dimensional morphological descriptors of angular and rounded limestone and basalt particles.

Descriptor	Limestone large		Limestone small		Basalt large		Basalt small	
	Angular	Rounded	Angular	Rounded	Angular	Rounded	Angular	Rounded
Circularity	0.825 ± 0.062	0.910 ± 0.046	0.842 ± 0.055	0.894 ± 0.043	0.863 ± 0.070	0.939 ± 0.033	0.899 ± 0.055	0.924 ± 0.047
Solidity	0.964 ± 0.014	0.987 ± 0.007	0.963 ± 0.016	0.979 ± 0.008	0.971 ± 0.009	0.984 ± 0.006	0.971 ± 0.009	0.977 ± 0.009
Convexity	0.984 ± 0.017	0.999 ± 0.002	0.988 ± 0.007	0.997 ± 0.005	0.989 ± 0.033	0.999 ± 0.002	0.995 ± 0.012	0.999 ± 0.005
Aspect ratio	1.561 ± 0.278	1.490 ± 0.266	1.480 ± 0.252	1.474 ± 0.215	1.445 ± 0.235	1.267 ± 0.158	1.395 ± 0.229	1.338 ± 0.194
Roundness	0.639 ± 0.108	0.683 ± 0.121	0.673 ± 0.120	0.677 ± 0.094	0.689 ± 0.107	0.786 ± 0.093	0.716 ± 0.106	0.746 ± 0.106

Note: Values are mean ± standard deviation. Circularity, solidity, convexity and roundness approach 1 as the projected particle geometry becomes more compact and regular; lower aspect ratio indicates reduced elongation.

The image-derived descriptors changed consistently after polishing. Circularity increased for all four combinations of aggregate type and particle size. Roundness increased and aspect ratio decreased in all four groups, although the magnitude of these changes depended on aggregate type and particle size. Solidity and convexity also increased in every group, indicating more convex and less irregular projected particle boundaries after polishing. Overall, these changes show that the modified drum polishing procedure produced more regular and compact projected particle geometries than the original, more angular particles. Because abrasive polishing may also alter surface texture and micro-roughness, these characteristics cannot be separated from the geometric modifications quantified by the two-dimensional descriptors. Accordingly, the CR–CA comparison is interpreted as a morphological contrast associated with angularity, rather than as an isolated effect of angularity.

2.4.Moisture Conditioning Procedures

Moisture-induced stripping was evaluated using two modified conditioning procedures for loose asphalt-coated aggregates, based on AASHTO T182 and ASTM D3625: static immersion and boiling water conditioning, respectively. Before mixing, the aggregate and binder were preheated to 135 °C for mixtures prepared with the neat binder and to 150 °C for mixtures prepared with the

SBS-modified binder. The heated aggregate was transferred to a metal pan on a hot plate, and 5.5 ± 0.2 g of binder was added per 100 ± 1 g of aggregate. The materials were then manually mixed for 2 min at the corresponding mixing temperature.

Each material combination was conditioned either in NaCl-free water or in a 4% NaCl solution. The NaCl medium was included to represent chloride-bearing moisture exposure relevant to winter de-icing and saline or coastal environments, rather than to reproduce a specific field de-icing solution concentration, because NaCl and other chloride-based solutions have been shown to affect asphalt–aggregate adhesion and moisture susceptibility [32–34].

For both conditioning procedures, the same specimen was evaluated sequentially at three observation stages. At each stage, specimens were removed from the conditioning medium, air-dried at room temperature for 24 h, and photographed under standardised imaging conditions. Except after the final observation, the specimens were then returned to their respective conditioning media. The reported conditioning durations refer to the cumulative exposure time in the conditioning medium and exclude the intermediate 24 h drying periods.

2.4.1. Static Immersion Test

The static immersion procedure was adapted from AASHTO T182. Asphalt-coated aggregate specimens were immersed in either NaCl-free water or a 4% NaCl solution and kept at 60 °C. Extended cumulative conditioning periods of 1, 3, and 7 days were used. Multiple water immersion durations have similarly been used in previous interfacial studies to characterise the progressive deterioration of asphalt–aggregate adhesion [35,36]. A representative static immersion setup and a conditioned specimen are shown in Figure 2.



(a) (b)

Fig. 2 Static immersion conditioning procedure: (a) experimental conditioning setup; (b) representative asphalt-coated aggregate after conditioning and 24 h room-temperature drying, prior to image acquisition

2.4.2. Boiling Water Test

The boiling water procedure was conducted as a modified form of ASTM D3625. The standard 10 min boiling period was retained as the first observation stage, and cumulative exposure times of 30 and 60 min were added. Previous studies have similarly investigated extended boiling durations and have shown that longer boiling times can increase the measured extent of asphalt coating loss [37,38].

Before each exposure interval, the asphalt-coated aggregate specimens were reheated to approximately 85 °C and then placed in either boiling NaCl-free water or a 4% NaCl solution. After the 10- and 30-min observations, the specimens were reheated and returned to the same conditioning medium, where exposure continued until the next cumulative stage. A representative boiling-water setup and conditioned specimen are shown in Figure 3.



(a) **(b)**

Fig. 3 Boiling water conditioning procedure: (a) conditioning setup; (b) representative asphalt-coated aggregate after conditioning and 24 h room-temperature drying, prior to image acquisition

2.5.Digital Image Processing, Stripping Quantification and Validation Procedure

Digital images were captured after each conditioning stage, following a 24-hour drying period at room temperature. This drying step removed residual surface moisture that could cause specular reflections and interfere with colour-based classification of the aggregate surfaces. All photographs were taken using the same smartphone and imaging settings, with the flash switched off. The smartphone was mounted in a fixed position above the specimen and kept perpendicular to the imaging plane. Specimens were placed in transparent Petri dishes on a white background and photographed under consistent lighting conditions.

Images were analysed in MATLAB using a custom image processing routine. Each RGB image was first cropped to retain the entire specimen region while excluding unnecessary surrounding areas. The cropped image was then converted from RGB to the CIELAB colour space using MATLAB's rgb2lab function. The resulting a^* and b^* chromatic channels were used together to classify visibly exposed aggregate surfaces, while the L^* channel was not included in the stripping classification rule.

The total visible aggregate area was identified independently from a greyscale representation of the image. A fixed greyscale intensity threshold was applied to distinguish the darker asphalt-coated aggregate particles from the white background. Internal gaps within the detected particle regions were subsequently filled, so that the resulting binary mask represented the total visible particle area available for stripping assessment.

After determining the total aggregate mask, visibly stripped regions were classified according to their chromatic characteristics in the a^* and b^* channels. Because limestone and basalt exhibited different surface colours under standardised imaging conditions, separate source-specific classification criteria were established using calibration images for each of the two aggregate sources. The calibration set comprised 12 images, six of limestone and six of basalt, selected independently from the 24-image validation dataset. For each aggregate source, one calibration image represented each combination of conditioning procedure and observation stage, thereby covering both procedures across all three stages. A pixel was classified as visibly exposed aggregate only when it met the prescribed criteria in both chromatic channels simultaneously. The numerical classification criteria were treated as calibration parameters specific to the source and imaging setup rather than as universal threshold values. Once established, the corresponding criteria were applied unchanged to all experimental images from the relevant aggregate source, with no image-specific adjustments.

The preliminary stripped-area mask was intersected with the total aggregate mask so that only pixels within visible particle regions contributed to the measurements. A morphological opening was subsequently applied using a disk-shaped structuring element with a radius of 2 pixels to remove small, isolated classifications and reduce local segmentation noise. The extent of visible stripping was calculated as:

$$SA = \frac{N_s}{N_t} \times 100 \quad (1)$$

where SA is the measured stripped area (%), N_s is the number of pixels classified as visibly exposed aggregate after masking and morphological post-processing, and N_t is the total number of pixels within the visible aggregate mask. The standardised image acquisition setup and a representative processing sequence, including the conditioned specimen, total aggregate mask, and detected stripped area mask, are shown in Figure 4. The main image processing steps and their implementation are summarised in Table 5.

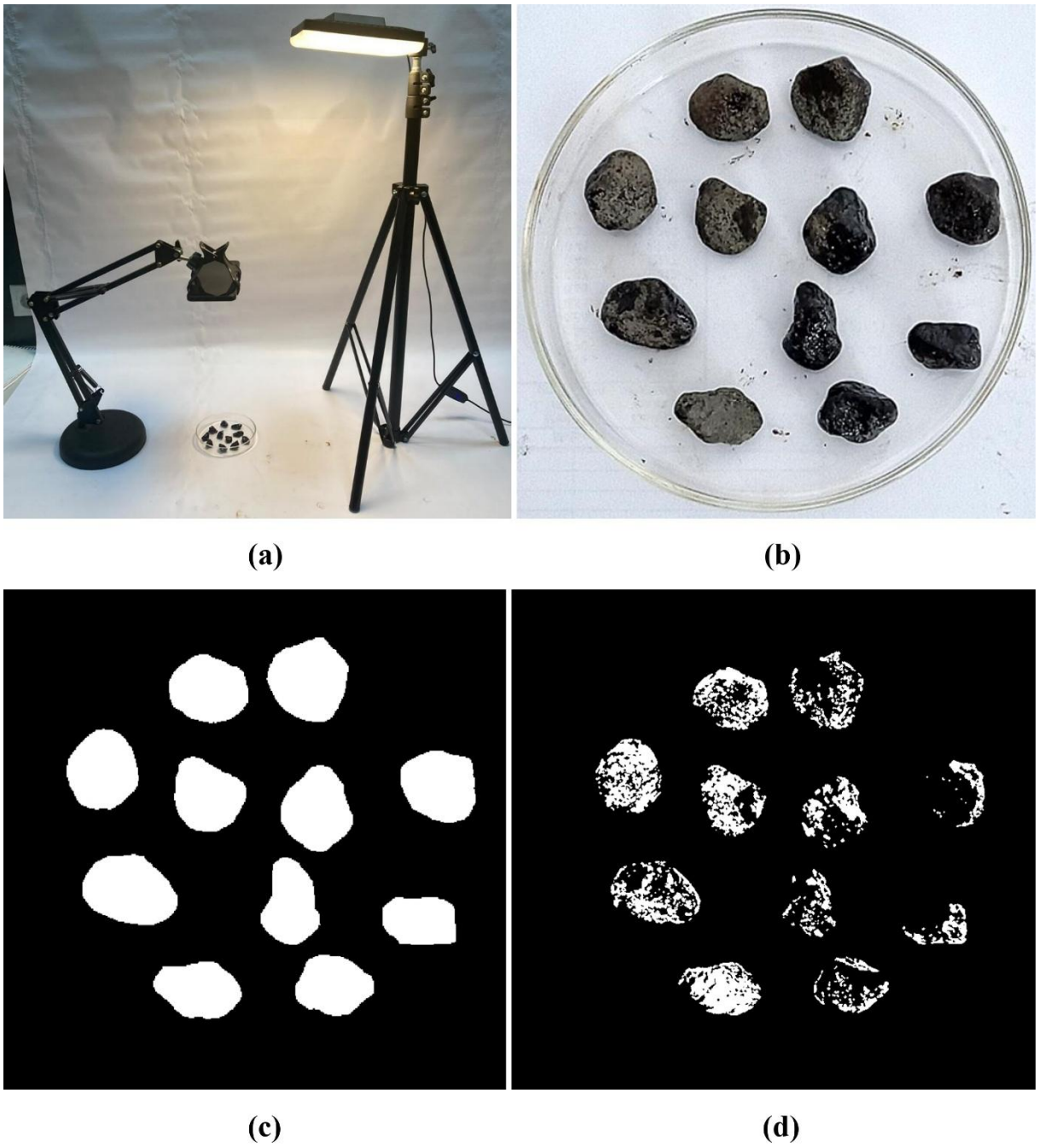


Fig. 4 Representative image processing and stripping-quantification procedure: (a) standardised smartphone imaging setup; (b) representative conditioned aggregate image; (c) binary aggregate mask defining the total visible aggregate area; and (d) corresponding binary mask of detected stripped areas

Table 5. Main steps of the image processing procedure used for stripping quantification.

Processing step	Implementation
Input	RGB digital photograph
Colour transformation	RGB → CIELAB using MATLAB rgb2lab
Classification channels	a^* and b^*
Classification logic	Simultaneous a^* AND b^* criteria
Total aggregate mask	Greyscale segmentation followed by hole filling
Aggregate-source treatment	Separately calibrated fixed criteria for limestone and basalt
Spatial restriction	Stripping mask intersected with total aggregate mask
Post-processing	Morphological opening
Structuring element	Disk, radius = 2 pixels
Output	Visible stripped pixels / total visible aggregate pixels × 100

The performance of the fixed, image-based measurement procedure was evaluated using a separate validation set of 24 conditioned images, independent of the images used for calibration. The validation dataset was balanced across aggregate source and conditioning procedure, comprising 12 limestone and 12 basalt images, and 12 static immersion and 12 boiling water conditioning images. For each conditioning procedure, four images represented each observation stage, comprising two limestone images and two basalt images.

Reference stripped-area masks were manually delineated by a single assessor using ImageJ. For each validation image, the assessor examined the original photograph and manually marked regions where visible loss of asphalt coating exposed the underlying aggregate. Reference delineation was performed directly on the original photographs, without viewing or using the corresponding MATLAB-generated masks as guidance.

Agreement between the reference and automated measurements was evaluated using the mean absolute error (MAE), mean bias, the Dice similarity coefficient, and Lin's concordance correlation coefficient (CCC). For each validation image i, the signed measurement error was defined as:

$$e_i = SA_{MATLAB,i} - SA_{ref,i} \quad (2)$$

where $S_{MATLAB,i}$ and $S_{ref,i}$ are the MATLAB-derived and reference stripped area percentages, respectively. MAE and mean bias were then calculated as:

$$MAE = \frac{1}{n}\sum_{i=1}^{n}|e_i| \quad (3)$$

and

$$Bias = \frac{1}{n}\sum_{i=1}^{n} e_i \quad (4)$$

where n is the number of validation images. Positive bias indicates systematic overestimation by the automated procedure, whereas negative bias indicates systematic underestimation by the same procedure.

Pixel-level spatial correspondence between the automated and reference classifications was evaluated using the Dice similarity coefficient:

$$Dice = \frac{2N_{TP}}{2N_{TP}+N_{FP}+N_{FN}} \quad (5)$$

where N_{TP} is the number of pixels classified as stripped in both the reference and automated masks, N_{FP} is the number classified as stripped only by the automated mask, and N_{FN} is the number classified as stripped only by the reference mask. The Dice coefficient was calculated separately for each validation image, and the resulting values were summarised as the mean ± standard deviation. The Dice coefficient therefore characterises spatial correspondence at the pixel level, whereas the CCC was used to assess concordance between the corresponding reference and MATLAB-derived stripped area percentages.

Finally, the original photographs and their corresponding automated binary masks were examined side by side as a quality-control step to identify any obvious segmentation failures. This inspection was performed only after the predetermined processing procedure had been applied and did not involve modifying the source-specific classification criteria or making image-specific adjustments to the segmentation parameters.

2.6.Statistical Analysis

The static immersion and boiling water datasets were analysed separately because the two procedures represent distinct conditioning regimes and were not intended to provide directly comparable absolute stripping values. To account for repeated measurements on the same experimental unit, population-averaged marginal models were fitted using generalised estimating equations (GEEs). A Gaussian distribution with an identity link function was specified for the stripped area response. Specimen identity was used as the clustering variable, conditioning duration was treated as a categorical within-specimen factor, and an unstructured working correlation matrix with robust sandwich standard errors was used.

The fixed explanatory variables were conditioning medium, binder system, ageing condition, aggregate type, particle size, and aggregate morphology. A binder system × ageing interaction was included to assess whether the ageing-related response differed between the two binder systems. Interactions between conditioning duration and conditioning medium, binder system, ageing condition, aggregate type, particle size, and aggregate morphology were included to evaluate whether the corresponding factor effects changed as conditioning progressed. These duration interactions were retained in both procedure-specific models. A duration × binder system × ageing interaction was also evaluated. This three-way interaction was retained for boiling-water conditioning, where the binder system × ageing interaction changed significantly across conditioning stages (Wald χ^2 (2) = 108.30, $p < 0.001$), but it was not retained for static immersion because the corresponding interaction was not significant (Wald χ^2 (2) = 3.75, $p = 0.153$).

Statistical significance was assessed using Wald tests with $\alpha = 0.05$. Because significant duration interactions indicated that the magnitude of most experimental factor effects depended on conditioning stage, factor effects were primarily interpreted using stage-specific adjusted marginal contrasts, averaged over the remaining experimental factors and expressed in percentage points (pp) with 95% confidence intervals. The overall effect of conditioning duration was evaluated using an omnibus Wald test, and adjusted marginal means were estimated for each conditioning stage. Because shape and angularity were not fully crossed, aggregate morphology was interpreted using the prespecified, stage-specific adjusted marginal contrasts for CR–CA and FA–CA, representing morphological comparisons related to angularity and shape, respectively. The duration dependence of these contrasts was evaluated using Wald tests. Full model specifications, coefficient estimates, working correlation structure, robust standard errors, interaction tests, conditioning-duration analyses, and stage-specific marginal contrasts are reported in Online Resource 1.

Cross-method associations were evaluated at nominally corresponding early, intermediate, and final observation stages (1 day versus 10 min, 3 days versus 30 min, and 7 days versus 60 min, respectively). These stage pairings were used solely to compare the relative differentiation of the same 96 treatment combinations between the two conditioning procedures and were not assumed to represent equivalent conditioning intensity. Pearson's correlation coefficient (r) was used to assess the linear association between stripped-area measurements obtained from the two procedures, and Spearman's rank correlation coefficient (ρ) was used to assess the similarity of the rankings of the 96 treatment combinations.

3. Results and Discussion

3.1. Performance of the Image-Based Stripping Measurement

After calibrating the source-specific segmentation criteria using separate images, the performance of the fixed image processing procedure was evaluated on 24 conditioned images from an independent validation set, covering both aggregate types, both conditioning procedures and all observation stages. Representative examples of the reference and automated classifications for limestone and basalt are shown in Figure 5.

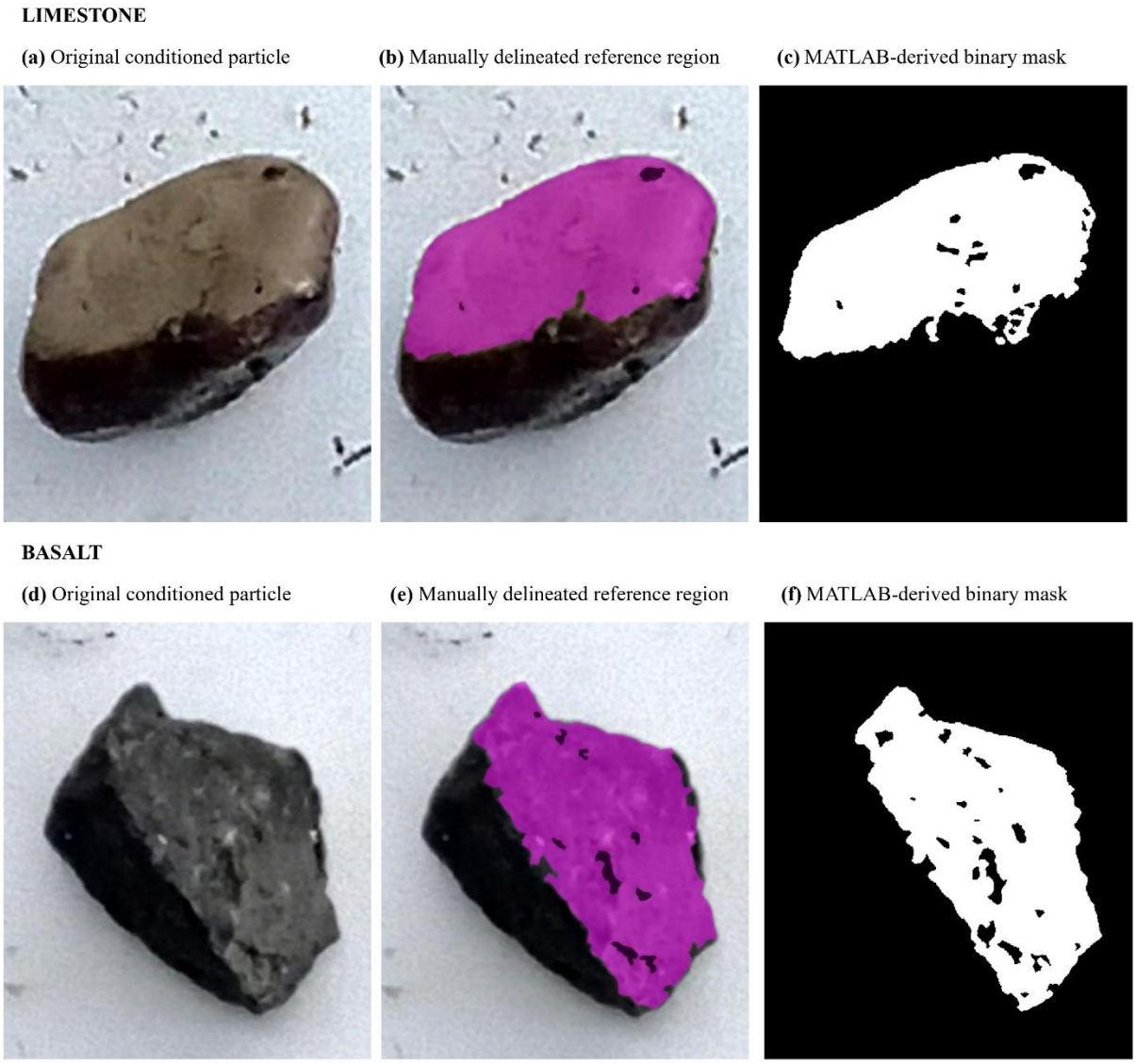


Fig. 5 Representative validation of the digital image processing procedure for limestone (a–c) and basalt (d–f): (a, d) original conditioned particles; (b, e) manually delineated reference regions; and (c, f) MATLAB-derived stripped area masks

Quantitative measurement performance is summarised in Table 6. For limestone, the procedure yielded a mean absolute error of 5.57 percentage points and a mean bias of +0.85 percentage points (pp), whereas for basalt the corresponding values were 3.78 pp and −1.44 pp.

Table 6. Validation performance of the image processing procedure.

Aggregate	n	MAE (pp)	Mean bias (pp)	Dice coefficient	CCC
Limestone	12	5.57	+0.85	0.927 ± 0.021	0.940
Basalt	12	3.78	−1.44	0.938 ± 0.028	0.958
Overall	24	4.68	−0.30	0.933 ± 0.025	0.946

Note: MAE = mean absolute error; pp = percentage points; CCC = Lin's concordance correlation coefficient. Mean bias represents the average of MATLAB-derived stripping minus reference stripping across the validation images. Dice coefficients are reported as mean ± standard deviation.

Across the full validation dataset, the CCC was 0.946, the overall MAE was 4.68 percentage points, and the overall mean bias was −0.30 percentage points. These results indicate strong agreement between the reference and MATLAB-derived stripped area percentages, with a relatively small overall systematic bias. The overall Dice coefficient was 0.933 ± 0.025, indicating strong spatial correspondence between the reference and the automated classifications. The individual paired reference and MATLAB-derived measurements are shown in Figure 6. This representation allows examination of the distribution of individual measurement deviations, rather than relying solely on the aggregate validation statistics shown in Table 6.

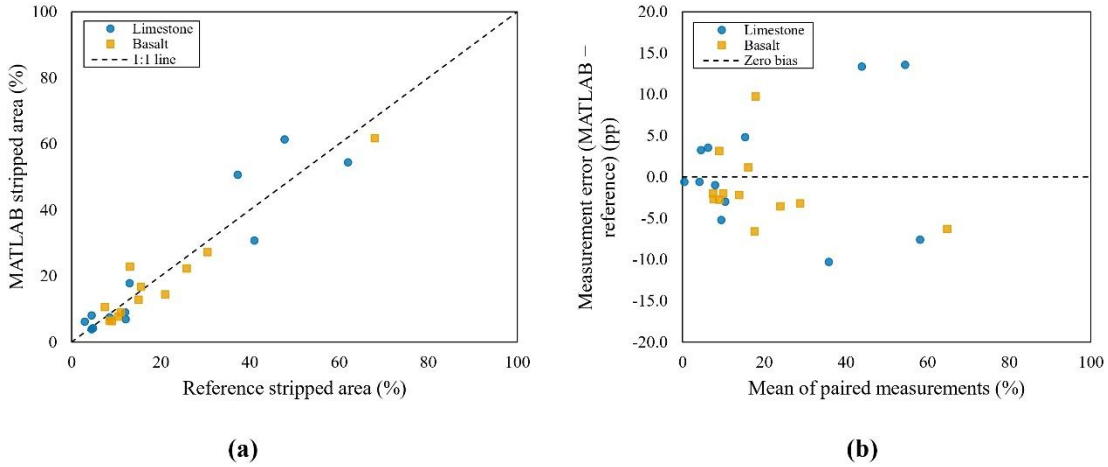


Fig. 6 Individual-level comparison of reference and MATLAB-derived stripped area measurements: (a) MATLAB-derived stripping versus reference stripping, with the dashed diagonal line representing perfect agreement; (b) measurement error (MATLAB − reference) versus the mean of the paired measurements. The horizontal dashed line represents zero bias; the overall mean bias was −0.30 pp

Taken together, the validation results support using the image processing procedure to quantitatively compare visible stripped area percentages across the examined materials and imaging conditions. Accordingly, the following analysis focuses on differences in the measured percentage of visible coating loss. Although several adjusted contrasts smaller than the image-level MAE were statistically significant because they were estimated systematically across the factorial

dataset, their small numerical magnitudes should not be interpreted as evidence of substantial practical separation between the material groups.

3.2.Overall Stripping Response and Effects of Conditioning Duration and Medium

Figure 7 shows that the stripped area increased progressively with conditioning duration under both procedures and in both conditioning media. The extended conditioning periods therefore captured a substantial progression of visible coating loss in both procedures. GEE analysis confirmed an overall effect of conditioning duration in both procedures ($p < 0.001$). The adjusted marginal mean stripped area increased from 5.12% at 1 day to 36.12% at 7 days during static immersion, and from 12.18% at 10 min to 48.96% at 60 min during boiling water conditioning (Online Resource 1).

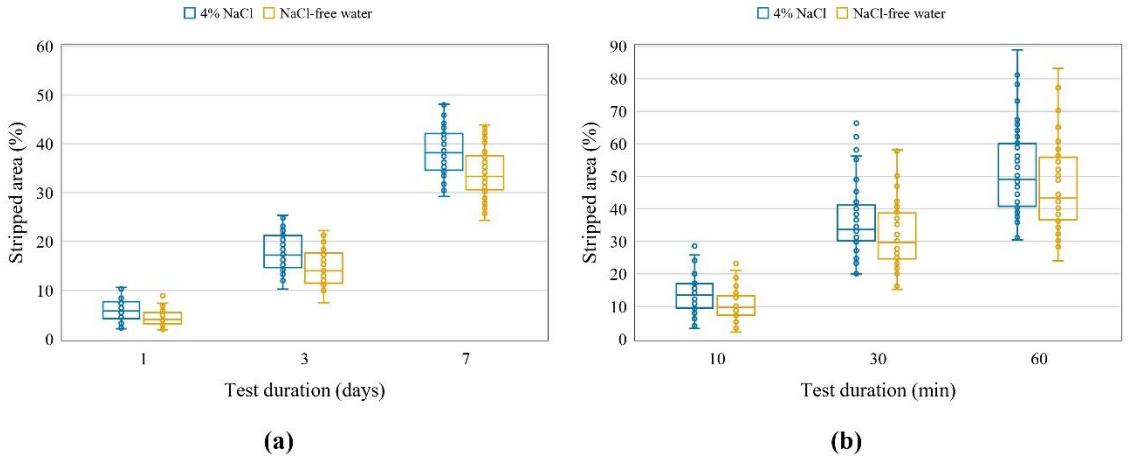


Fig. 7 Distribution of stripped area with conditioning duration under 4% NaCl and NaCl-free water conditions: (a) static immersion; (b) boiling water conditioning. Boxes represent the interquartile range, centre lines indicate the median and individual points represent the observed stripped area values

Conditioning in 4% NaCl caused more stripping than conditioning in NaCl-free water in both procedures, and the magnitude of this difference increased with conditioning duration. During static immersion, the adjusted difference between 4% NaCl and NaCl-free water increased from 1.62 percentage points after 1 day to 3.31 percentage points after 3 days and 4.24 percentage points after 7 days. The duration × conditioning medium interaction was significant (Wald χ^2 (2) = 138.08, $p < 0.001$), confirming that the effect of NaCl changed as conditioning progressed. During boiling-water conditioning, the corresponding adjusted differences were 2.86 percentage points at 10 min, 4.63 percentage points at 30 min, and 5.31 percentage points at 60 min, with a significant duration × conditioning medium interaction (Wald χ^2 (2) = 20.01, $p < 0.001$). These results indicate that the difference between NaCl-containing and NaCl-free conditioning became more pronounced as exposure duration increased in both procedures. This finding is consistent with previous studies

showing that NaCl and other chloride-based solutions can affect asphalt–aggregate adhesion and moisture susceptibility under relevant exposure conditions [32–34,39].

The progression of stripping as a function of conditioning duration differed descriptively between the two procedures. Under both conditioning media, the greatest increase during boiling water conditioning occurred between 10 and 30 min, whereas during static immersion it occurred between 3 and 7 days. These differences should be interpreted in the context of the distinct conditioning regimes, rather than as evidence that stripping progressed more rapidly in one of the procedures. Boiling water conditioning rapidly exposes materials to high temperatures, and previous studies have shown that the measured extent of stripping increases with boiling duration [37,38]. By comparison, progressive deterioration of asphalt–aggregate adhesion has been observed over several days of water immersion [35,36]. Because moisture-induced deterioration of asphalt–aggregate adhesion depends on both conditioning duration and temperature [40], the exposure times used in the two procedures cannot be regarded as equivalent measures of conditioning severity. The two procedures are therefore better compared in terms of the progression of stripping and the relative material differentiation within each conditioning regime, rather than by directly comparing absolute stripped area values.

3.3.Effects of Binder System and Ageing

Figure 8 shows how the binder system and ageing affect the stripped area. The neat binder consistently exhibited greater stripping than the SBS-modified binder under both ageing conditions and conditioning procedures. During static immersion, the adjusted difference between the neat and SBS-modified binder systems increased from 2.69 percentage points (pp) after 1 day to 4.65 pp after 3 days and 5.78 pp after 7 days. The duration × binder system interaction was significant (Wald χ^2 (2) = 191.41, $p < 0.001$), indicating that the magnitude of the binder system difference increased as conditioning progressed. During boiling water conditioning, the corresponding adjusted differences were 6.74 pp at 10 min, 14.10 pp at 30 min, and 16.03 pp at 60 min. For boiling water conditioning, the adjusted binder system contrast also varied significantly across conditioning stages (Wald χ^2 (2) = 298.54, $p < 0.001$).

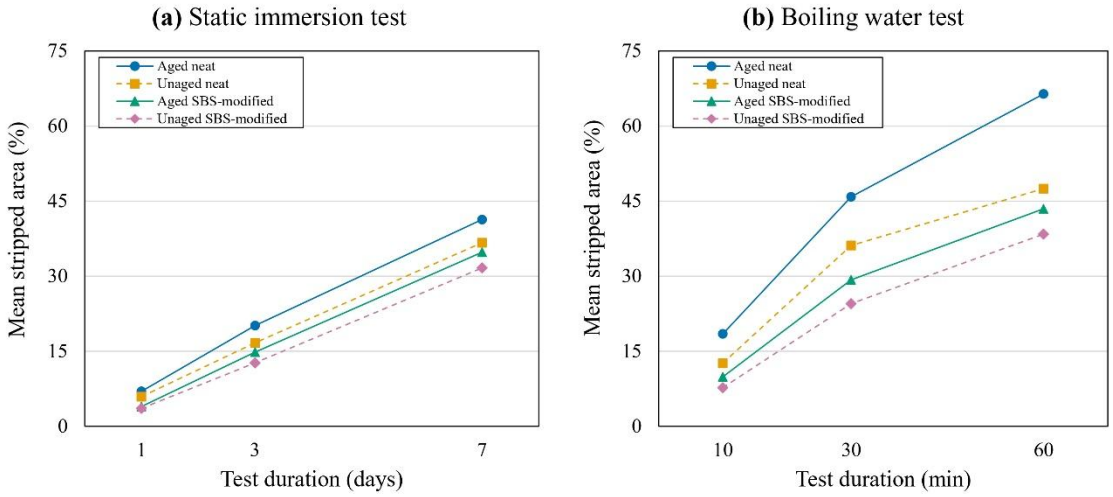


Fig. 8 Mean stripped area with conditioning duration for the neat 50/70 and SBS-modified PG 76-16 binder systems under unaged and RTFO-aged conditions: (a) static immersion test; (b) boiling water test

The reduced stripping observed for the SBS-modified binder is consistent with previous studies reporting improved moisture resistance in SBS-modified asphalt mixtures [16]. Previous research has shown that SBS modification can alter binder rheology and elasticity [15], and can influence binder cohesion, asphalt–aggregate adhesion, and moisture susceptibility, depending on the binder–aggregate combinations used [14]. However, the two binders investigated here were distinct binder systems rather than unmodified and SBS-modified variants of a single base binder. The observed difference in coating retention therefore cannot be attributed specifically to SBS modification and may reflect the combined effects of polymer modification, binder grade, binder composition, rheological properties, and other formulation differences between the two binder systems.

Binder ageing also significantly affected coating loss, and the ageing-related difference increased with conditioning duration. During static immersion, the adjusted difference between RTFO-aged and unaged binder systems increased from 0.72 percentage points (pp) after 1 day to 2.78 pp after 3 days and 3.88 pp after 7 days. The duration × ageing interaction was significant (Wald χ^2 (2) = 203.40, $p < 0.001$), indicating that the ageing effect became more pronounced as conditioning progressed. During boiling water conditioning, the corresponding adjusted differences were 4.01 pp at 10 min, 7.26 pp at 30 min, and 11.99 pp at 60 min. For boiling water conditioning, the adjusted ageing contrast also varied significantly across conditioning stages (Wald χ^2 (2) = 213.30, $p < 0.001$).

Previous studies have similarly shown that binder ageing can increase the potential for asphalt–aggregate debonding and reduce resistance to moisture damage [17,19]. Xiao and Huang further demonstrated that the effect of ageing depends on whether the binder is aged before coating the aggregate or after it comes into contact with the aggregate surface [17]. Liu et al. also reported

increased stripping with longer binder ageing times using a modified boiling water procedure [38]. Because this study quantified visible coating loss rather than binder chemistry or interfacial energy, the specific mechanisms responsible for the ageing effect cannot be determined directly from these data.

During static immersion, the adjusted difference in the ageing-associated response between the neat and SBS-modified binder systems was 1.12 percentage points (pp; 95% CI 0.45–1.79; p = 0.001). However, there was no evidence that the binder system × ageing interaction itself changed with conditioning duration (duration × binder system × ageing: Wald χ^2 (2) = 3.75, p = 0.153).

In contrast, during boiling-water conditioning, the binder system × ageing interaction changed markedly as conditioning time increased. The adjusted difference in the ageing-associated response between the two binder systems increased from 3.68 pp at 10 min to 4.97 pp at 30 min and 13.86 pp at 60 min, with a significant duration × binder system × ageing interaction (Wald χ^2 (2) = 108.30, $p < 0.001$). At the final 60 min stage, ageing increased mean stripping by 18.93 pp for the neat binder system, compared with 5.06 pp for the SBS-modified binder system. Guo et al. [41] reported a similar trend, observing greater resistance to age-related deterioration of asphalt–aggregate adhesion in an SBS-modified asphalt system than in an unmodified asphalt system.

3.4.Effects of Aggregate Type and Particle Size

The effects of aggregate type and particle size on the stripped area are shown in Figure 9. Basalt consistently exhibited greater stripping than limestone under both conditioning procedures, and the magnitude of this difference increased with conditioning duration. During static immersion, the adjusted basalt–limestone difference increased from 1.64 percentage points (pp) at 1 day to 4.06 pp at 3 days and 4.94 pp at 7 days. The interaction between duration and aggregate type was significant (Wald χ^2 (2) = 234.27, $p < 0.001$), indicating that the effect of aggregate type became more pronounced as conditioning progressed. During boiling water conditioning, the corresponding adjusted differences were 4.64 pp at 10 min, 7.33 pp at 30 min, and 10.55 pp at 60 min. The interaction between duration and aggregate type was also significant for boiling water conditioning (Wald χ^2 (2) = 114.54, $p < 0.001$).

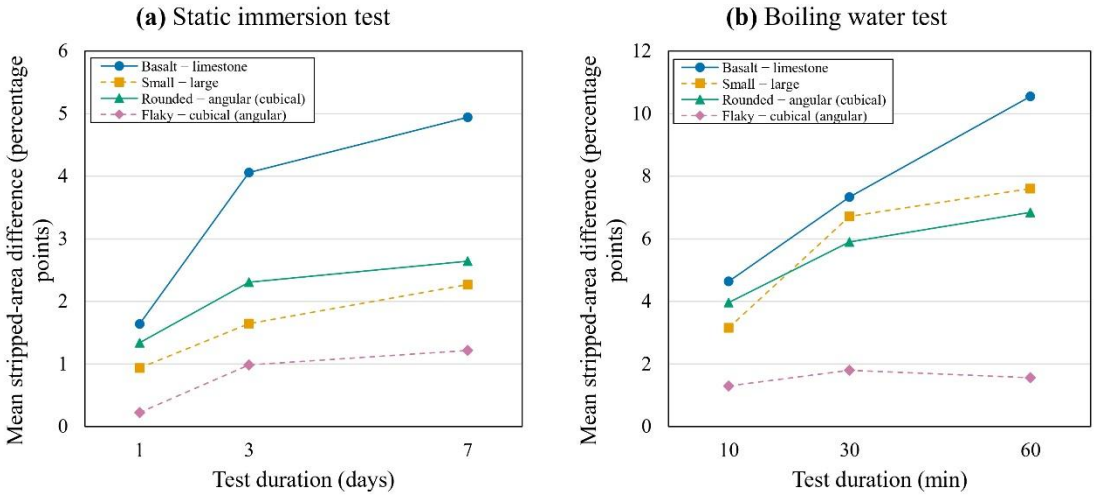


Fig. 9 Descriptive mean differences in stripped area associated with aggregate characteristics as a function of conditioning duration: (a) static immersion test; (b) boiling water test

The lower level of stripping observed in limestone is consistent with previous evidence that the mineralogical composition and physicochemical characteristics of the aggregate can substantially influence asphalt–aggregate adhesion and moisture susceptibility [7,8]. Based on surface energy characterisation and a modified boiling water test with imaging, Chen et al. reported that limestone exhibited stronger adhesion and greater resistance to moisture-induced stripping than basalt [9]. The difference between basalt and limestone observed here may therefore reflect source-dependent variations in mineralogical and physicochemical characteristics, rather than aggregate type alone. Because aggregate mineralogy and surface energy were not directly characterised in the present study, the specific interfacial mechanisms responsible for this difference cannot be identified from the available data.

Particle size also significantly affected stripping, and the magnitude of this effect increased with conditioning duration. During static immersion, the adjusted difference between small and large particles increased from 0.94 percentage points (pp) at 1 day to 1.64 pp at 3 days and 2.27 pp at 7 days. The interaction between duration and particle size was significant (Wald χ^2 (2) = 34.52, $p < 0.001$), indicating that the effect of particle size became more pronounced as conditioning progressed. During boiling water conditioning, the corresponding adjusted differences were 3.16 pp at 10 min, 6.71 pp at 30 min, and 7.61 pp at 60 min. The duration × particle size interaction was also significant for boiling water conditioning (Wald χ^2 (2) = 68.81, $p < 0.001$).

At the constant binder-to-aggregate mass ratio used in this study, the smaller particle fraction would generally provide a larger total surface area for coating, which could reduce the average asphalt film thickness and contribute to greater loss of coating. This interpretation is consistent with Khodaii et al., who reported increased stripping potential as aggregate size decreased [12]. Sengoz and Agar also demonstrated that asphalt film thickness affects the moisture susceptibility of asphalt mixtures [42]. However, because aggregate surface area and asphalt film thickness were

not directly measured in the present study, this explanation should be regarded as a plausible contributing mechanism rather than an experimentally verified cause.

3.5.Effects of Aggregate Morphology

Among cubical particles, rounded aggregates consistently exhibited greater stripping than angular aggregates, and the magnitude of the CR–CA difference increased with conditioning duration. During static immersion, the adjusted CR–CA contrast increased from 1.34 percentage points (pp) after 1 day to 2.31 pp after 3 days and 2.64 pp after 7 days. The duration × morphology interaction for the CR–CA contrast was significant (Wald χ^2 (2) = 27.71, $p < 0.001$), indicating that the difference between cubical-rounded and cubical-angular particles became more pronounced as conditioning progressed. During boiling water conditioning, the corresponding adjusted differences were 3.96 pp at 10 min, 5.90 pp at 30 min, and 6.85 pp at 60 min. The duration dependence of the CR–CA contrast was also significant for boiling water conditioning (Wald χ^2 (2) = 17.89, $p < 0.001$).

However, the treatment did not only alter angularity. Los Angeles abrasion has been shown to reduce aggregate angularity and surface texture complexity, while physical abrasion also reduces surface micro-roughness [43,44]. These changes are relevant because increased angularity and rougher surface texture have been associated with improved asphalt–aggregate adhesion [45]. Accordingly, the CR–CA comparison is best interpreted as a morphological contrast related to angularity, which may also involve changes in surface texture, rather than as the isolated effect of angularity alone.

The FA–CA contrast was smaller in magnitude than the CR–CA contrast. During static immersion, the adjusted difference between flaky–angular and cubical–angular particles increased from 0.22 pp at 1 day to 0.99 pp at 3 days and 1.22 pp at 7 days. The 1-day FA–CA contrast was not statistically significant (95% CI −0.08 to 0.53; $p = 0.150$), whereas the differences at 3 and 7 days were statistically significant. This indicates that the distinction between flaky–angular and cubical–angular particles became apparent only after further static immersion conditioning. During boiling water conditioning, the corresponding FA–CA contrasts were 1.30 pp at 10 min, 1.80 pp at 30 min, and 1.56 pp at 60 min. All three stage-specific contrasts were significant ($p = 0.002$, 0.015, and 0.035, respectively); however, the magnitude of the FA–CA contrast did not change significantly with boiling duration (Wald χ^2 (2) = 0.49, $p = 0.782$).

Previous studies have also linked aggregate shape to moisture resistance. Mohammad et al. reported lower TSR and IRS values as the proportion of flat and elongated particles increased [13], whereas Qian et al. observed improved moisture resistance with increasing aggregate sphericity in porous asphalt mixtures [46].

3.6.Relative Magnitude of the Investigated Factor Effects

Because the effects of most experimental factors varied significantly with conditioning duration, their relative magnitudes were compared using stage-specific adjusted marginal contrasts rather

than contrasts averaged across all observation stages. As shown in Online Resource 1, the binder system contrast produced the largest adjusted material difference at every conditioning stage in both procedures. Overall, these results show that the magnitudes of the investigated material and conditioning effects depend on the exposure stage. Stage-specific contrasts are therefore more informative than duration-averaged estimates for characterising how material differentiation progresses. These comparisons apply only to the factor levels and conditioning stages investigated and should not be interpreted as a universal ranking of the importance of the material factors. In addition, because the static immersion and boiling water models were fitted separately, differences in contrast magnitude between the two procedures should not be interpreted as formal statistical comparisons between conditioning methods.

3.7.Cross-Method Association and Limitations

The static immersion and boiling water procedures showed strong positive associations in the responses to the corresponding treatment combinations. As shown in Table 7, Pearson correlation coefficients ranged from 0.879 to 0.910 across the early, intermediate, and final observation stages, while Spearman rank correlation coefficients ranged from 0.888 to 0.911; all correlations were significant at $p < 0.001$. However, these correlations should not be interpreted as evidence of agreement or equivalence between the two methods. The paired observation stages represent corresponding early, intermediate, and final phases rather than equivalent conditioning severities, and the procedures differed substantially in temperature, duration, and exposure conditions. The correlations therefore indicate consistency in relative material differentiation rather than interchangeability of the measured stripped area values.

Table 7. Cross-method correlations in stripped area at corresponding observation stages.

Observation stage	Static immersion	Boiling water test	Pearson r	Spearman ρ
Early	1 day	10 min	0.903	0.903
Intermediate	3 days	30 min	0.879	0.888
Final	7 days	60 min	0.910	0.911

Note: Each correlation was based on 96 corresponding treatment combinations. All correlations were significant at $p < 0.001$.

Nevertheless, the findings should be interpreted in the context of the limitations of the experimental design and measurement procedures. Each treatment combination was represented by a single experimental unit measured repeatedly; therefore, the factorial design allows estimation of average factor effects but does not provide independent replication to assess repeatability within each treatment combination. Shape and angularity were not fully crossed because a flaky-rounded condition was unavailable, and the polishing treatment may also have altered the surface texture. The broader applicability of the findings is also limited because only two aggregate types, two binder systems, and a single NaCl concentration were investigated. The image processing procedure quantifies visible surface stripping but does not directly assess internal moisture damage, interfacial characteristics, or mechanical behaviour. Reference masks were delineated by a single assessor, so inter-observer variability was not assessed. Finally, validation was limited to 24 images

acquired using a single standardised imaging setup, and measurement performance with other cameras, lighting conditions, and image acquisition systems remains to be established.

Because specimens were removed and air-dried for 24 h between observation stages and, during boiling-water conditioning, reheated before subsequent exposure intervals, the modified procedures represent interrupted cumulative conditioning rather than continuous standard exposure. These interruptions may have influenced the progression of stripping. In addition, the neat 50/70 and SBS-modified PG 76-16 binders were distinct binder systems; therefore, differences associated with the binder system cannot be attributed specifically to SBS modification.

4. Conclusions

This study developed and independently evaluated an image-based framework for quantitatively measuring visible moisture-induced stripping, then applied the resulting standardised measurement procedure to characterise material and conditioning effects in two factorial experiments. The measurements showed strong agreement with manually delineated reference masks, with a concordance correlation coefficient of 0.946, a mean absolute error of 4.68 percentage points (pp), an overall mean bias of −0.30 pp, and a Dice coefficient of 0.933 ± 0.025. These results support using the procedure to quantitatively compare visible coating loss under the standardised imaging conditions investigated, while small material contrasts should be interpreted in the context of the observed image-level measurement error.

Progressive conditioning increased visible coating loss in both procedures, while the adjusted effect of 4% NaCl, relative to NaCl-free water, increased from 1.62 to 4.24 pp during static immersion and from 2.86 to 5.31 pp during boiling water conditioning.

Among the material contrasts investigated, the binder system showed the greatest adjusted difference at every stage of conditioning. Ageing-related differences also increased with conditioning duration, with particularly pronounced differentiation between the two binder systems during extended conditioning in boiling water.

Aggregate characteristics also produced systematic differences in measured coating loss. Basalt exhibited greater stripping than limestone, smaller particles stripped more than larger ones, and the difference between cubical-rounded and cubical-angular particles increased with conditioning duration in both procedures. The contrast between flaky-angular and cubical-angular particles was smaller and showed a less consistent dependence on conditioning duration.

Static immersion and boiling water conditioning produced similar relative differentiation among the 96 material combinations. However, this consistency should not be interpreted as quantitative equivalence between the two conditioning approaches.

The principal contribution of this study is the integration of independent measurement validation with systematic material characterisation. The procedure remains specific to the imaging conditions and aggregate sources investigated, and broader transferability should be established through independent replication, additional aggregate–binder systems, multiple imaging configurations, and complementary mechanical and interfacial measurements.

References

[1] Little DN, Jones DR (2003) Chemical and mechanical processes of moisture damage in hot-mix asphalt pavements. In: Moisture sensitivity of asphalt pavements: a national seminar. Transportation Research Board, San Diego, California, pp 37–70

[2] Bhasin A, Little DN, Vasconcelos KL, Masad E (2007) Surface free energy to identify moisture sensitivity of materials for asphalt mixes. Transp Res Rec 2001:37–45. https://doi.org/10.3141/2001-05

[3] Bhasin A, Masad E, Little D, Lytton R (2006) Limits on adhesive bond energy for improved resistance of hot-mix asphalt to moisture damage. Transp Res Rec 1970:2–13. https://doi.org/10.1177/0361198106197000101

[4] Brondani C, Faccin C, Specht LP, Nummer AV, da Silva Pereira D, Vestena PM, Baroni M (2023) Evaluation of moisture susceptibility of asphalt mixtures: influence of aggregates, visual analysis, and mechanical tests. J Mater Civ Eng 35:04022433. https://doi.org/10.1061/(ASCE)MT.1943-5533.0004603

[5] Howson J, Masad E, Bhasin A, Little D, Lytton R (2011) Comprehensive analysis of surface free energy of asphalts and aggregates and the effects of changes in pH. Constr Build Mater 25:2554–2564. https://doi.org/10.1016/j.conbuildmat.2010.11.098

[6] Lucas Júnior JLO, Babadopulos LFAL, Soares JB (2019) Aggregate–binder adhesiveness assessment and investigation of the influence of morphological and physico-chemical properties of mineral aggregates. Road Mater Pavement Des 20:S79–S94. https://doi.org/10.1080/14680629.2019.1588773

[7] Zhang J, Apeagyei AK, Airey GD, Grenfell JR (2015) Influence of aggregate mineralogical composition on water resistance of aggregate–bitumen adhesion. Int J Adhes Adhes 62:45–54. https://doi.org/10.1016/j.ijadhadh.2015.06.012

[8] Gaudenzi E, Cardone F, Lu X, Canestrari F (2022) Performance assessment of asphalt mixtures produced with a bio-binder containing 30% of lignin. Mater Struct 55:221. https://doi.org/10.1617/s11527-022-02057-w

[9] Chen L, Li J, Xiang H, Zhang J, Feng E, Kong L (2025) Effect of aggregate type on asphalt–aggregate adhesion and its quantitative characterization. Materials 18:3696. https://doi.org/10.3390/ma18153696

[10] Huang T, Luo J, Luo R, Tu C (2022) Investigation on the relationship between the surface texture index and the surface free energy of aggregate. Constr Build Mater 325:126759. https://doi.org/10.1016/j.conbuildmat.2022.126759

[11] Kuang D, Wang X, Jiao Y, Zhang B, Liu Y, Chen H (2019) Influence of angularity and roughness of coarse aggregates on asphalt mixture performance. Constr Build Mater 200:681–686. https://doi.org/10.1016/j.conbuildmat.2018.12.176

[12] Khodaii A, Haghshenas HF, Tehrani HK (2012) Effect of grading and lime content on HMA stripping using statistical methodology. Constr Build Mater 34:131–135. https://doi.org/10.1016/j.conbuildmat.2012.02.025

[13] Mohammad HK, Albayati AH, Al-Kheetan MJ (2025) Influence of coarse aggregate geometry and mineral composition on the durability of asphalt concrete. Infrastructures 10:263. https://doi.org/10.3390/infrastructures10100263

[14] Hu J, Zhang L, Zhang X, Guo Y, Yu XB (2020) Comparative evaluation of moisture susceptibility of modified/foamed asphalt binders combined with different types of aggregates using surface free energy approach. Constr Build Mater 256:119429. https://doi.org/10.1016/j.conbuildmat.2020.119429

[15] Lu X, Isacsson U (1997) Rheological characterization of styrene-butadiene-styrene copolymer modified bitumens. Constr Build Mater 11:23–32. https://doi.org/10.1016/S0950-0618(96)00033-5

[16] Gorkem C, Sengoz B (2009) Predicting stripping and moisture induced damage of asphalt concrete prepared with polymer modified bitumen and hydrated lime. Constr Build Mater 23:2227–2236. https://doi.org/10.1016/j.conbuildmat.2008.12.001

[17] Xiao R, Huang B (2022) Moisture damage mechanism and thermodynamic properties of hot-mix asphalt under aging conditions. ACS Sustain Chem Eng 10:14865–14887. https://doi.org/10.1021/acssuschemeng.2c04786

[18] Bionghi RBK, Amani S, Shahraki D, Karimi MM (2025) Characterizing the effects of aging and modification on asphalt binder bonding properties and moisture sensitivity. Case Stud Constr Mater 23:e05351. https://doi.org/10.1016/j.cscm.2025.e05351

[19] Al Basiouni Al Masri Z, Alarab A, Chehab G, Tehrani-Bagha A (2019) Assessing moisture damage of asphalt-aggregate systems using principles of thermodynamics: effects of recycled materials and binder aging. J Mater Civ Eng 31:04019190. https://doi.org/10.1061/(ASCE)MT.1943-5533.0002846

[20] Amelian S, Abtahi SM, Hejazi SM (2014) Moisture susceptibility evaluation of asphalt mixes based on image analysis. Constr Build Mater 63:294–302. https://doi.org/10.1016/j.conbuildmat.2014.04.012

[21] Jameel MS, Khan AH, Kahlid B, Raza A, Zaidi SBA, Ali B, Ouni MHE (2023) MATLAB image analysis approach for adhesion and moisture susceptibility assessment of modified asphalt concrete. Constr Build Mater 402:133025. https://doi.org/10.1016/j.conbuildmat.2023.133025

[22] Sahari Moghaddam A, Rezazadeh Azar E, Mejias Y, Bell H (2020) Estimating stripping of asphalt coating using k-means clustering and machine learning–based classification. J Comput Civ Eng 34:04019044. https://doi.org/10.1061/(ASCE)CP.1943-5487.0000864

[23] Xiao R, Polaczyk P, Huang B (2022) Measuring moisture damage of asphalt mixtures: the development of a new modified boiling test based on color image processing. Measurement 190:110699. https://doi.org/10.1016/j.measurement.2022.110699
[24] Chen S, Tong D, Zhang Q, Wu X (2024) Evaluation of adhesion between styrene-butadiene-styrene (SBS) modified asphalt and aggregates based on rolling bottle test and image processing. Constr Build Mater 431:136531. https://doi.org/10.1016/j.conbuildmat.2024.136531
[25] Wang W, Li C, Zhao X, Song P, Li J, Zheng J, Bu S, Wang X (2024) An image-based method for evaluating changes in particle size and morphology distributions of aggregate materials after vibratory compaction test. Constr Build Mater 430:136483. https://doi.org/10.1016/j.conbuildmat.2024.136483
[26] Xiao R, Polaczyk P, Wang Y, Ma Y, Lu H, Huang B (2022) Measuring moisture damage of hot-mix asphalt (HMA) by digital imaging-assisted modified boiling test (ASTM D3625): recent advancements and further investigation. Constr Build Mater 350:128855. https://doi.org/10.1016/j.conbuildmat.2022.128855
[27] Lantieri C, Lamperti R, Simone A, Vignali V, Sangiorgi C, Dondi G, Magnani M (2017) Use of image analysis for the evaluation of rolling bottle tests results. Int J Pavement Res Technol 10:45–53. https://doi.org/10.1016/j.ijprt.2016.11.003
[28] Subramaniam DN, Dassanayake DHHP, Ahilash N, Wijekoon SHB, Sathiparan N (2024) Characterisation of the shape of aggregates using image analysis. Int J Pavement Eng 25:2349905. https://doi.org/10.1080/10298436.2024.2349905
[29] Al-Rousan T, Masad E, Tutumluer E, Pan T (2007) Evaluation of image analysis techniques for quantifying aggregate shape characteristics. Constr Build Mater 21:978–990. https://doi.org/10.1016/j.conbuildmat.2006.03.005
[30] Szmańda JB, Witkowski K (2021) Morphometric parameters of Krumbein grain shape charts—a critical approach in light of the automatic grain shape image analysis. Minerals 11:937. https://doi.org/10.3390/min11090937
[31] Zhu X, Serati M, Asche H, Yang X (2026) Grain-scale insights into crushed waste glass as a sustainable fine aggregate. Mater Struct 59:121. https://doi.org/10.1617/s11527-026-03013-8
[32] Fakhri M, Javadi S, Sedghi R, Arzjani D, Zarrinpour Y (2019) Effects of deicing agents on moisture susceptibility of the WMA containing recycled crumb rubber. Constr Build Mater 227:116581. https://doi.org/10.1016/j.conbuildmat.2019.07.307
[33] Ye Z, Zhang X, Zhang Z, Qiao F, Luo R, Zhou L, Li X (2026) Analysis of asphalt and asphalt-aggregate interface eroded by salt ions: MD simulation and composition investigation. Mater Struct 59:64. https://doi.org/10.1617/s11527-026-02949-1
[34] Wu Z, Shi C, Gao P, Zhang H, Hu X (2023) Moisture susceptibility of asphalt mixture subjected to chloride-based deicing salt solutions under simulated environmental conditions. J Mater Civ Eng 35:04023052. https://doi.org/10.1061/(ASCE)MT.1943-5533.0004713
[35] Cala A, Caro S, Lleras M, Rojas-Agramonte Y (2019) Impact of the chemical composition of aggregates on the adhesion quality and durability of asphalt-aggregate systems. Constr Build Mater 216:661–672. https://doi.org/10.1016/j.conbuildmat.2019.05.030

[36] Cui S, Blackman BR, Kinloch AJ, Taylor AC (2014) Durability of asphalt mixtures: effect of aggregate type and adhesion promoters. Int J Adhes Adhes 54:100–111. https://doi.org/10.1016/j.ijadhadh.2014.05.009
[37] Bhargava N, Undela NR, Nanda H, Siddagangaiah AK, Ryntathiang TL (2021) Utilizing photodetection technique to assess moisture damage of asphalt mixtures. J Mater Civ Eng 33:04021311. https://doi.org/10.1061/(ASCE)MT.1943-5533.0003937
[38] Liu X, Chen S, Ma T, Wu X, Yang J (2023) Investigation of adhesion property between asphalt binder and aggregate using modified boiling methods for hot and wet area. J Mater Civ Eng 35:04022467. https://doi.org/10.1061/(ASCE)MT.1943-5533.0004646
[39] Zhou Z, Li H, Liu X, He W (2020) Investigation of sea salt erosion effect on the asphalt-aggregate interfacial system. Int J Pavement Res Technol 13:145–153. https://doi.org/10.1007/s42947-019-0095-2
[40] Gong Y, Xu J, Yan EH (2021) Intrinsic temperature and moisture sensitive adhesion characters of asphalt-aggregate interface based on molecular dynamics simulations. Constr Build Mater 292:123462. https://doi.org/10.1016/j.conbuildmat.2021.123462
[41] Guo M, Yin X, Du X, Tan Y (2023) Effect of aging, testing temperature and relative humidity on adhesion between asphalt binder and mineral aggregate. Constr Build Mater 363:129775. https://doi.org/10.1016/j.conbuildmat.2022.129775
[42] Sengoz B, Agar E (2007) Effect of asphalt film thickness on the moisture sensitivity characteristics of hot-mix asphalt. Build Environ 42:3621–3628. https://doi.org/10.1016/j.buildenv.2006.10.006
[43] Kuang D, Zhang B, Jiao Y, Fang J, Chen H, Wang L (2017) Impact of particle morphology on aggregate-asphalt interface behavior. Constr Build Mater 132:142–149. https://doi.org/10.1016/j.conbuildmat.2016.11.132
[44] Ji X, Chen Y, Hou Y, Dai C, Chen B, Zou H (2021) Surface microscopic properties of various aggregates using laser scanning confocal microscope. Constr Build Mater 290:123222. https://doi.org/10.1016/j.conbuildmat.2021.123222
[45] Cui P, Xiao Y, Yan B, Li M, Wu S (2018) Morphological characteristics of aggregates and their influence on the performance of asphalt mixture. Constr Build Mater 186:303–312. https://doi.org/10.1016/j.conbuildmat.2018.07.124
[46] Qian Z, Ren H, Wei Y (2021) Effect of aggregate gradation and morphology on porous asphalt mixture performance. J Mater Civ Eng 33:04021055. https://doi.org/10.1061/(ASCE)MT.1943-5533.0003655

Acknowledgements

The authors would like to thank the Department of Civil Engineering at Manisa Celal Bayar University for providing laboratory facilities and technical support during the experimental phase of this research.

Author contributions

Yalcin Karakaya: Conceptualization, Methodology, Software, Investigation, Formal analysis, Data curation, Visualization, Writing – original draft. Ayhan Oner Yucel: Conceptualization, Methodology, Software, Investigation, Formal analysis, Data curation, Visualization, Writing – review and editing. Dilay Yildirim Uncu: Conceptualization, Formal analysis.

Statements and Declarations

Data availability

The data that support the findings of this study are available from the corresponding author upon reasonable request.

Funding

The authors did not receive support from any organization for the submitted work.

Competing interests

The authors have no relevant financial or non-financial interests to disclose.

Supplementary Information

Online Resource 1: GEE model specifications, coefficient estimates, conditioning-duration inference, and stage-specific adjusted marginal contrasts.

Supplementary Files

This is a list of supplementary files associated with this preprint. Click to download.

- ESM1.xlsx